



**HAL**  
open science

# Stability Analysis of Bio-inspired Source Seeking with Noisy Sensors

I Rañó, Mehdi Khamassi, K Wong-Lin

► **To cite this version:**

I Rañó, Mehdi Khamassi, K Wong-Lin. Stability Analysis of Bio-inspired Source Seeking with Noisy Sensors. 2021 European Control Conference (ECC), Jul 2021, Kongens Lyngby, Denmark. hal-03277526

**HAL Id: hal-03277526**

**<https://hal.science/hal-03277526>**

Submitted on 3 Jul 2021

**HAL** is a multi-disciplinary open access archive for the deposit and dissemination of scientific research documents, whether they are published or not. The documents may come from teaching and research institutions in France or abroad, or from public or private research centers.

L'archive ouverte pluridisciplinaire **HAL**, est destinée au dépôt et à la diffusion de documents scientifiques de niveau recherche, publiés ou non, émanant des établissements d'enseignement et de recherche français ou étrangers, des laboratoires publics ou privés.

# Stability Analysis of Bio-inspired Source Seeking with Noisy Sensors

I. Rañó<sup>1</sup> and M. Khamassi<sup>2</sup> and K. Wong-Lin<sup>3</sup>

**Abstract**—Braitenberg vehicles have been used for decades to implement source seeking and avoidance behaviours in bio-inspired robotics. Recently, new theoretical results have derived convergence conditions of these bio-inspired controllers under the assumption of noiseless sensors. Although Braitenberg vehicles have been experimentally shown to work in outdoor scenarios, there is no theoretical evidence that shows they also can work in perceptually harsh environments. In this paper we mathematically analyse the source seeking behaviour of Braitenberg vehicle 3a with noisy sensors, when noise cannot be ignored. We approximate the stimulus the vehicle is seeking close to a source and derive the evolution equations for the average and covariance of the trajectory realisations. The analysis of the resulting non-linear differential equations shows that, under some conditions, the average trajectory is convergent and the dispersion around this trajectory is bounded. We illustrate these theoretical results through simulations, but also show that our results extend to general source seeking situations where the approximations do not hold.

## I. INTRODUCTION

Animals and humans can perform tasks in harsh environments, highly dynamic environments which induce perception or action discontinuities and present high levels of perceptual noise. For instance, one can safely drive a car under rain or foggy condition – up to some extent – and cope with the visual uncertainty weather conditions create. While conventional robotic sensors (e.g. range sensors) might be unreliable in harsh environments, unconventional and experimental sensing modalities like; electrosense, chemical or thermal sensing, pressure sensing et cetera, suffer from non-negligible effects like hysteresis, sensing delays and noise even in mild environments. Since sensor effects like delays and noise can turn stable closed-loop controllers unstable [1], extending the stability results of source seeking to the case of noisy sensors is far from trivial. In this paper we show that Braitenberg vehicles can lead to stable source seeking behaviour in the presence of perceptual noise. Specifically, we analyse the behaviour of our drift-diffusion model of Braitenberg vehicles [2] in the vicinity of a source point and show that the dispersion of the trajectories can be bounded if the controller is selected appropriately.

Braitenberg vehicles are qualitative models of bio-inspired sensor-based local navigation displaying source seeking and avoidance behaviours [3]. They can be quantitatively modelled as a family of non-linear controllers for wheeled robots

[4], but they have been shown to work for snake-like [5] and fish-like [6] robots. Using these quantitative models [4] it can be shown that source seeking and avoidance trajectories appear as solutions to the closed-loop system of non-linear differential equations. Moreover, one can obtain stability conditions like global stability for isotropic stimuli [7], conditional stability, and oscillatory behaviour [8]. All these theoretical results assume noiseless sensors (or the existence of a potential function), yet, as we will see below, multiple works successfully used Braitenberg vehicles in real robots in scenarios where noise cannot be ignored. Therefore, empirical works have shown that this source seeking mechanism works in practice, but key issues like stability limits have not been explored. In this paper we focus on vehicle 3a, the source seeking model shown in figure 1, for which a stochastic closed-loop model as a drift-diffusion equation was presented in [2].

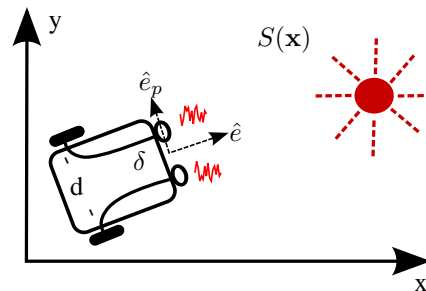


Fig. 1. Braitenberg vehicle 3a with sensor noise

One of the first works in robot based chemical source seeking [9] successfully applied Braitenberg vehicles 3a and 3b to perform chemotaxis. This experimental analysis used two symmetrically placed chemical sensors to approach areas of high concentrations of chemicals. Besides dealing with noise and air turbulence, this work showed that this bio-inspired controller can deal with slow sensor dynamics [10]. Several works also used Braitenberg vehicles to implement robotic phonotaxis, i.e. sound source seeking. In a series of papers [11], [12], [13] the motion of female crickets towards the male chirping was replicated in robots. A spiking neural network combined vehicles 2a and 3b to control the movement of the robot wheels using increasing and decreasing dynamic connections, showing an excellent performance even in outdoor environments. The work presented in [14] proposes the design of a pinnea for a rat robot and implements phonotaxis through a model of the central auditory system of rats and a vehicle 3a. Another implementation of phonotaxis relying on Braitenberg vehicle 2b [15] uses instead a model of the auditory system of

<sup>1</sup>I. Rañó is with SDU Biorobotics, University of Southern Denmark, Denmark. e-mail: igr@mmmi.sdu.dk

<sup>2</sup>M. Khamassi is with the Institut des Systèmes Intelligents et de Robotique, Sorbonne Université, France. e-mail: mehdi.khamassi@upmc.fr

<sup>3</sup>K.F. Wong-Lin is with the Intelligent Systems Research Centre, Ulster University, UK. e-mail: k.wong-lin@ulster.ac.uk

lizards to detect pre-defined frequencies. In these phonotaxis implementations, sensor noise or noise in the signal derived from the sound cannot be ignored, yet Braitenberg vehicles showed good performance. Besides chemical and sound sensing the principles of Braitenberg vehicles have been used in underwater robotics with unconventional sensors. A fish-like robot with electrosense avoiding isolating objects and approaching conductive objects was presented in [16]. Given the experimental nature of this sensing modality sensor readings are obtained with relatively high levels of noise, which did not hamper their implementation of movement towards conductive objects.

Multiple experimental works have shown that Braitenberg vehicles can perform source reaching behaviours with real (noisy) sensors. Moreover, it has been also shown that navigation functions (in our case noisy stimuli) including noise terms can allow obstacle avoidance mechanism to escape local minima [17]. Although theoretical results show the convergence of Braitenberg vehicle 3a with noiseless sensors, adding noise to the sensors can change the stability properties [8] of this bio-inspired controller. The contribution of this paper is to theoretically show that this control mechanism can generate stable trajectories even in the presence of noise in the sensors. To find the stability conditions, the dynamics of the average and covariance of the trajectories of the stochastic differential equation modelling vehicle 3a are obtained as a set of non-linear ordinary differential equations. These equations describing a Braitenberg vehicle 3a close to a stimulus source can lead to stable trajectories with bounded covariance, i.e. a stable equilibrium point. The rest of the paper is organised as follows. Section II reviews the model, derives the analytical equations for the evolution of the first and second moments of the distribution of the vehicle under a parabolic stimulus, and shows that they can lead to stable trajectories. Section III presents simulations to illustrate the theoretical results, and some more general simulations that, although do not match the theoretical assumptions, show a similar long term behaviour. Section IV ends the paper presenting the conclusions and future lines of work.

## II. STOCHASTIC MODEL OF BRAITENBERG VEHICLES

This section reviews the derivation of the system of stochastic differential equations modelling Braitenberg vehicle 3a. Let us assume a non-negative smooth scalar stimulus  $S(\mathbf{x})$  in a domain  $\mathcal{D}$ . Braitenberg vehicle 3a has two symmetrically placed sensors controlling the speed on the corresponding wheel on the same side as shown in figure 1. We denote the connection or control function  $F(s)$ , which for vehicle 3a should be decreasing, i.e.  $F'(s) < 0$  for all the values  $s$  returned by the sensors. We assume a stimulus value with noise  $\eta$  with a variance smoothly dependent on the measured stimulus value  $\eta = \sigma(s)dW_t$ , where  $W_t$  is a Wiener process. The noise in general may be different for each sensor but we will assume it has the same statistical properties. Under these assumptions, for a vehicle with the left and right sensors located at  $\mathbf{x}_l$ , and  $\mathbf{x}_r$  respectively, the speed of the right and left wheels are  $v_r = F(S(\mathbf{x}_r) +$

$\sigma(S(\mathbf{x}_r))dW_t^r$ ) and  $v_l = F(S(\mathbf{x}_l) + \sigma(S(\mathbf{x}_l))dW_t^l)$ , where  $dW_t^l$  and  $dW_t^r$  are the independent noise processes on the left and right sensors. Considering the distance between the sensors is  $\delta$ , we can approximate  $v_l$  and  $v_r$  as Taylor series around the middle point between the sensors  $\mathbf{x}$ . Obtaining the forward speed and turning rate from these approximations and substituting them into the unicycle kinematic model we get the following closed-loop system of stochastic differential equations (see [2] for more details):

$$\begin{aligned} dx_t &= F(\mathbf{x}_t) \cos \theta_t dt + \frac{1}{2} D_1(\mathbf{x}_t, \theta_t) \cos \theta_t (dW_t^l + dW_t^r) \\ &\quad + \frac{1}{2} D_2(\mathbf{x}_t, \theta_t) \cos \theta_t (dW_t^l - dW_t^r) \\ dy_t &= F(\mathbf{x}_t) \sin \theta_t dt + \frac{1}{2} D_1(\mathbf{x}_t, \theta_t) \sin \theta_t (dW_t^l + dW_t^r) \\ &\quad + \frac{1}{2} D_2(\mathbf{x}_t, \theta_t) \sin \theta_t (dW_t^l - dW_t^r) \\ d\theta_t &= -\frac{\delta}{d} \nabla F(\mathbf{x}_t) \cdot \hat{\mathbf{e}}_p(\theta_t) dt - \frac{1}{d} D_1(\mathbf{x}_t, \theta_t) (dW_t^l - dW_t^r) \\ &\quad - \frac{1}{d} D_2(\mathbf{x}_t, \theta_t) (dW_t^l + dW_t^r) \end{aligned} \quad (1)$$

where  $d$  is the wheelbase of the vehicle,  $\hat{\mathbf{e}}_p = [-\sin \theta, \cos \theta]^T$  and the diffusion terms  $D_1(\mathbf{x}, \theta)$  and  $D_2(\mathbf{x}, \theta)$  are:

$$\begin{aligned} D_1(\mathbf{x}, \theta) &= \frac{\delta^2}{4} F''(\mathbf{x}) \sigma(\mathbf{x}) [\nabla S(\mathbf{x}) \cdot \hat{\mathbf{e}}_p]^2 + F'(\mathbf{x}) \sigma(\mathbf{x}) \\ D_2(\mathbf{x}, \theta) &= \frac{\delta}{2} \nabla S(\mathbf{x}) \cdot \hat{\mathbf{e}}_p [F'(\mathbf{x}) \sigma'(\mathbf{x}) + F''(\mathbf{x}) \sigma(\mathbf{x})] \end{aligned} \quad (2)$$

where to simplify the expressions we use the following notation;  $F(\mathbf{x}_t) = F(S(\mathbf{x}_t))$ ,  $F'(\mathbf{x}_t) = F'(S(\mathbf{x}_t))$ , and so on. The diffusion terms depend on the noise variance  $\sigma(s)$ , the control function  $F(s)$ , and their derivatives. They correspond to non-additive noise as the terms multiplying the increments of the Wiener processes,  $dW_t^r$  and  $dW_t^l$ , have a functional dependency on  $\mathbf{x}_t$  and  $\theta_t$ . There is no way of turning these terms into additive noise because of the effect of the trigonometric functions of the angular variable in the first two equations of the system (1).

The system of equations (1) describes the time evolution of a Braitenberg vehicle 3a with noisy sensors immersed into an environment with stimulus  $S(\mathbf{x})$ . The drift terms are equivalent to the deterministic model which leads to an equilibrium point  $\mathbf{x}^*$  if  $F(S(\mathbf{x}^*)) = 0$  and  $\nabla S(\mathbf{x}^*) = \mathbf{0}$ . These deterministic equations correspond to a non-linear differential equation for which some analytical solutions can be found under several assumptions. One such analytical solution corresponds to the case of parabolic symmetry (i.e.  $S(\mathbf{x}^T A \mathbf{x})$ ) of the stimulus, which leads to straight line trajectories when the vehicle is directly heading towards the source along the principal axis of the parabola. This, in turn, allows linearising the motion equations and analysing the evolution and stability of nearby trajectories. As we will see below, this analysis can be extended to the case of noisy sensors.

### A. Approximations of the first two moments of the trajectories

This section derives the equations of the evolution of the average trajectory and the covariance matrix of the trajectory realisations from the system of stochastic differential equations (1) modelling Braitenberg vehicle 3a in closed-loop. If we consider the general form of a stochastic differential equation  $d\mathbf{x}_t = \mathbf{f}(\mathbf{x}_t)dt + \mathbf{g}(\mathbf{x}_t)d\mathbf{W}_t$ , where  $\mathbf{x}_t \in \mathbb{R}^n$  is an  $n$  dimensional stochastic process;  $d\mathbf{W}_t \in \mathbb{R}^m$  is an  $m$  dimensional uncorrelated white Gaussian noise; and  $\mathbf{f} : \mathbb{R}^n \rightarrow \mathbb{R}^n$  and  $\mathbf{g} : \mathbb{R}^n \rightarrow \mathbb{R}^n \times \mathbb{R}^m$  are respectively vector and matrix functions, the equations for the average trajectories can be obtained taking expectations on both sides of the equation. Since  $E[\mathbf{g}(\mathbf{x}_t)d\mathbf{W}_t] = \mathbf{0}$ , the equation for the average becomes  $d\boldsymbol{\mu}_x = E[\mathbf{f}(\mathbf{x}_t)]dt$ . If  $\mathbf{f}(\mathbf{x}_t)$  is a non-linear function its expectation can be computed using different approximations. A first order approximation leads to  $E[\mathbf{f}(\mathbf{x}_t)] = \mathbf{f}(E[\mathbf{x}_t])$ . In the case of equations (1), a second order approximation leads to the following system of non-linear differential equations:

$$\begin{aligned}\dot{\mu}_x &= F(\boldsymbol{\mu}_{xy}) \cos \mu_\theta + \frac{1}{2}tr(H_x \Sigma) \\ \dot{\mu}_y &= F(\boldsymbol{\mu}_{xy}) \sin \mu_\theta + \frac{1}{2}tr(H_y \Sigma) \\ \dot{\mu}_\theta &= -\frac{\delta}{d} \left[ \nabla F(\boldsymbol{\mu}_{xy}) \cdot \hat{e}_p(\mu_\theta) + \frac{1}{2}tr(H_\theta \Sigma) \right] \quad (3)\end{aligned}$$

where  $\boldsymbol{\mu}_{xy}$  is the vector of expectations  $[E[x_t], E[y_t]]^T$ , and  $\mu_\theta = E[\theta_t]$ ;  $\Sigma$  is the covariance matrix of  $x$ ,  $y$  and  $\theta$ , and  $H_x$ ,  $H_y$ , and  $H_\theta$  are the Hessian matrices of the  $x$ ,  $y$  and  $\theta$  components of the functional vector flow defined by  $[F(\mathbf{x}) \cos \theta, F(\mathbf{x}) \sin \theta, -\frac{\delta}{d} \nabla F(\mathbf{x}) \cdot \hat{e}_p]^T$  evaluated at the average  $\mu_x$ ,  $\mu_y$  and  $\mu_\theta$  (see [2]). It is worth noting that a first order approximation of the expectation of equations (1), i.e. discarding second order terms, leads to the deterministic equations of motion for this vehicle. However, equations (3) are more accurate since they are derived from a second order approximation.

The derivation of the evolution of the second moment, the covariance matrix, is more involved but in the general case of a stochastic differential equation  $d\mathbf{x}_t = \mathbf{f}(\mathbf{x}_t)dt + \mathbf{g}(\mathbf{x}_t)d\mathbf{W}_t$ , it is described by the differential matrix equation:

$$\dot{\Sigma} = J\mathbf{f}(\boldsymbol{\mu}_x)\Sigma + \Sigma J\mathbf{f}(\boldsymbol{\mu}_x)^T + \mathbf{g}(\boldsymbol{\mu}_x)\mathbf{g}(\boldsymbol{\mu}_x)^T \quad (4)$$

where  $J\mathbf{f}(\mathbf{x})$  is the Jacobian matrix of  $\mathbf{f}(\mathbf{x})$ , and  $\boldsymbol{\mu}_x$  is the average of the state vector.

### B. Moments of the vehicle under Parabolic stimuli

In this section we assume the stimulus  $S(\mathbf{x})$  has parabolic shape, or can be approximated as a parabola close to the maximum, which is possible if  $S(\mathbf{x})$  is at least of class  $C^2$ . Without loss of generality we will assume the maximum is located at the origin. Therefore, the stimulus function can be stated as  $S(\mathbf{x}) = g_0 - \frac{1}{2}\mathbf{x}^T A \mathbf{x}$  where  $A$  is a positive definite matrix. It is worth noting that this approximation works in general close to a stimulus source. For instance, light follows the inverse square law  $S(\mathbf{x}) \propto \frac{I_0}{h^2 + \|\mathbf{x}\|^2}$ , and

it can be approximated as  $S(\mathbf{x}) \propto \frac{I_0}{h^2} - \frac{I_0}{h^4}\|\mathbf{x}\|^2$ . We can further assume that the matrix  $A$  is diagonal with elements  $a_{11}$  and  $a_{22}$  in the diagonal, or rotate our reference system to be aligned with the eigenvectors of  $A$ . To simplify the noise terms we will also assume that the noise in the sensors is additive, i.e.  $\sigma(\mathbf{x}) = \sigma_0$  with  $\sigma_0$  constant, and the control function is linear or can be approximated linearly around  $s_0 = S(\mathbf{0})$ ,  $F(s) = \alpha(g'_0 - s)$ , where the controller parameters  $\alpha$  and  $g'_0$  are real positive numbers. It is worth noting that when  $g'_0 = g_0$  the drift part of equations (1) – equivalent to the deterministic model – has an equilibrium point at the origin as  $F(S(\mathbf{x})) = \alpha\mathbf{x}^T A \mathbf{x}$ , when  $g'_0 > g_0$  there is no equilibrium point, and when  $g'_0 < g_0$  there is an elliptic region of equilibrium points around the origin. Because  $F'(s) = -\alpha$ , the diffusion terms are  $D_1(\mathbf{x}, \theta) = -\alpha\sigma_0$  and  $D_2(\mathbf{x}, \theta) = 0$ .

We want to analyse the stability of the stochastic system close to the equilibrium point of the deterministic model, i.e. checking whether the equilibrium point of the deterministic system still appears in the case of noisy sensors. The analysis of the first order approximation of the average trajectory  $E[\mathbf{f}(\mathbf{x}_t)] = \mathbf{f}(E[\mathbf{x}_t])$  reduces to the analysis of the deterministic case [8] as mentioned above. In this case the vehicle follows a straight line trajectory approaching the maximum when the initial position of the vehicle lays along the principal axis defined by the matrix  $A$  and it directly heads towards the source. Although this is also true for the first order approximation of the average trajectory, the second order approximation, equation (3), depends on terms containing the evolution of the covariance matrix, i.e.  $tr(H_x \Sigma)$ ,  $tr(H_y \Sigma)$  and  $tr(H_\theta \Sigma)$ , which could make the average trajectory deviate from a straight line. The covariance matrix, in turn, evolves according to equation (4). If we denote  $\Sigma = (\sigma_{ij})$  with  $i, j = x, y, \theta$ , and since  $\sigma_{ij} = \sigma_{ji}$ , the evolution of the average trajectory for the stimulus approximate close to the source is given by:

$$\begin{aligned}\dot{\mu}_x &= \alpha \left[ \frac{1}{2} \left( 1 - \frac{\sigma_{\theta\theta}}{2} \right) \boldsymbol{\mu}_{xy}^T A \boldsymbol{\mu}_{xy} + (g'_0 - g_0) \right] \cos \mu_\theta \\ &\quad + \frac{\alpha}{2} (a_{11}\sigma_{xx} + a_{22}\sigma_{yy}) \cos \mu_\theta \\ &\quad - \alpha (a_{11}\sigma_{x\theta}\mu_x + a_{22}\sigma_{y\theta}\mu_y) \sin \mu_\theta \\ \dot{\mu}_y &= \alpha \left[ \frac{1}{2} \left( 1 - \frac{\sigma_{\theta\theta}}{2} \right) \boldsymbol{\mu}_{xy}^T A \boldsymbol{\mu}_{xy} + (g'_0 - g_0) \right] \sin \mu_\theta \\ &\quad + \frac{\alpha}{2} (a_{11}\sigma_{xx} + a_{22}\sigma_{yy}) \sin \mu_\theta \\ &\quad + \alpha (a_{11}\sigma_{x\theta}\mu_x + a_{22}\sigma_{y\theta}\mu_y) \cos \mu_\theta \\ \dot{\mu}_\theta &= -\alpha \frac{\delta}{d} \left[ \left( 1 - \frac{\sigma_{\theta\theta}}{2} \right) \boldsymbol{\mu}_{xy}^T A \hat{e}_p(\mu_\theta) \right. \\ &\quad \left. + \frac{\delta}{d} (a_{11}\sigma_{x\theta} \cos \mu_\theta + a_{22}\sigma_{y\theta} \sin \mu_\theta) \right] \quad (5)\end{aligned}$$

Our aim is to analyse the solution of these equations when the vehicle starts with a pose that generates straight line trajectories in the deterministic system, since they have analytical solution. That starting pose corresponds to  $(\mu_x(0), \mu_y(0), \mu_\theta(0)) = (-d, 0, 0)$  with  $d > 0$  while the initial conditions of the covariance matrix corresponds to

$\Sigma(0) = 0$ . If we compute the dynamics of the covariance matrix, eq. (4), for the vehicle and consider these initial conditions we get that the equations for the evolution of  $\sigma_{xy}$  and  $\sigma_{x\theta}$  are;  $\dot{\sigma}_{xy} = 0$  and  $\dot{\sigma}_{x\theta} = 0$ . Since the initial values of the covariance matrix are zeros, the terms on equations (5) containing  $\sigma_{xy}$  and  $\sigma_{x\theta}$  will vanish. Moreover, since  $\mu_{xy} = (-d, 0)$  and  $\hat{e}_p = (0, 1)$  the equation for the average angle evolution becomes  $\dot{\mu}_\theta = 0$ , which means  $\mu_\theta(t) = 0$ , so there is no change in the average orientation of the vehicle. It can be seen that the evolution equation for the  $y$  average also vanishes, i.e.  $\dot{\mu}_y = 0$ , and therefore we only need to consider the evolution of  $\mu_x$ . This means that the average trajectory for the stochastic differential equation (1) under parabolic stimulus with a second order approximate of the average behaves similarly to the deterministic case. Specifically, the evolution of the average  $x$  position,  $\mu_x$ , is given by:

$$\begin{aligned} \dot{\mu}_x = & \alpha(g'_0 - g_0) + \frac{1}{2}\alpha [a_{11}\sigma_{xx} + a_{22}\sigma_{yy}] \\ & + \frac{\alpha a_{11}}{2} \left[ 1 - \frac{\sigma_{\theta\theta}}{2} \right] \mu_x^2 \end{aligned} \quad (6)$$

where the evolution of the non zero elements of the covariance matrix  $\sigma_{xx}$ ,  $\sigma_{yy}$ ,  $\sigma_{\theta\theta}$ , and  $\sigma_{y\theta}$  can be derived from equation (4). Using the initial conditions above and the fact that the average angle is constant,  $\mu_\theta(t) = 0$ , the evolution of these elements of  $\Sigma$  can be stated as:

$$\begin{aligned} \dot{\sigma}_{xx} = & \frac{\alpha^2 \sigma_0^2}{2} + 2a_{11}\mu_x\sigma_{xx} \\ \dot{\sigma}_{yy} = & 2\alpha(g'_0 - g_0)\sigma_{y\theta} + \alpha a_{11}\sigma_{y\theta}\mu_x^2 \\ \dot{\sigma}_{y\theta} = & -\alpha a_{22}\frac{d}{\delta}\sigma_{yy} + \alpha(g'_0 - g_0)\sigma_{\theta\theta} + \alpha a_{11}\frac{d}{\delta}\sigma_{y\theta}\mu_x \\ & + \frac{1}{2}\alpha a_{11}\sigma_{\theta\theta}\mu_x^2 \\ \dot{\sigma}_{\theta\theta} = & \frac{2\alpha^2 \sigma_0^2}{d^2} - 2\frac{d}{\delta}\alpha a_{22}\sigma_{y\theta} + 2\frac{d}{\delta}a_{11}\alpha\sigma_{\theta\theta}\mu_x \end{aligned} \quad (7)$$

where it is worth noting that  $\sigma_{y\theta}$  is not zero, so there is a correlation between the deviation from the straight line trajectory ( $y(t) = 0$ ) and the angular variable  $\theta$ .

Equations (6) and (7) form a system of non-linear differential equations that approximate the evolution of the moments of the trajectories of Braitenberg vehicle 3a with noisy sensors starting with a pose  $(-d, 0, 0)$ . Finding the equilibrium points of this system is not trivial, but some conclusions can be drawn by analysing the structure of the equations. First, it is worth reminding that all the parameters ( $\delta$ ,  $d$ ,  $\alpha$ ,  $a_{11} \dots$ ) are positive reals, and the variables  $\sigma_{xx}$ ,  $\sigma_{yy}$  and  $\sigma_{\theta\theta}$  should be also positive. On the other hand,  $\sigma_{y\theta}$  could be negative, while  $\mu_x < 0$  because of the initial pose of the vehicle (although it might become possible if the vehicle passes the source). By first analysing the equation for  $\dot{\sigma}_{xx}$  we can see that  $\sigma_{xx}$  will have a stable equilibrium point as long as the vehicle does not reach the source, i.e.  $\mu_x < 0$ , meaning that the dispersion of the trajectories along the  $x$  axis will be bounded. However, if the average trajectories reach the origin  $\mu_x = 0$ , the variance  $\sigma_{xx}$  will increase linearly over time. This divergence on  $\sigma_{xx}$  could occur for values of  $\mu_x$  close to the source if the term  $\frac{\alpha^2 \sigma_0^2}{2}$  is large enough.

The evolution of the other components of the covariance matrix, equations (7), is more complex to analyse as the potential equilibrium points depend on the sign of  $\sigma_{y\theta}$  and the values of the parameters of the stimulus and the linear control function. For instance,  $\sigma_{yy}$  could have an equilibrium point if  $\sigma_{y\theta} < 0$ , but also if  $g'_0 < g_0$ . In the case of the angular covariance  $\sigma_{\theta\theta}$ , a negative value of  $\sigma_{y\theta}$  would make  $\sigma_{\theta\theta}$  increase, yet it could have a stable equilibrium point as long as the average  $x$  coordinate  $\mu_x$  is negative as the last term of the dynamic equation would be negative. Finally, the large amount of terms with different signs on the evolution equation of  $\sigma_{y\theta}$  makes its analysis complicated. However, it cannot be ruled out that  $\sigma_{y\theta}$  takes negative values making the equation for  $\sigma_{yy}$  stable. In any case it might be possible to find a combination of parameters that bound  $\sigma_{xx}$ ,  $\sigma_{yy}$  and  $\sigma_{\theta\theta}$ .

We can also analyse the evolution of the average  $x$  position, equation (6). This again is a combination of positive and negative terms which can lead to a stable equilibrium point, i.e. the final average position of the vehicle. While the terms on  $\sigma_{xx}$  and  $\sigma_{yy}$  are positive, the last term can change its sign depending on the value of  $\sigma_{\theta\theta}$ . This could lead to a stable equilibrium point, but also the constant term  $\alpha(g'_0 - g_0)$  could lead to stability as long as  $g'_0 < g_0$ . Trying to simultaneously solve equations (6) and (7) to find the equilibrium point, i.e.  $\dot{\mu}_x = 0$ ,  $\dot{\sigma}_{xx} = 0$ ,  $\dot{\sigma}_{yy} = 0$ ,  $\dot{\sigma}_{y\theta} = 0$  and  $\dot{\sigma}_{\theta\theta} = 0$ , leads to a high degree polynomial with complex solutions dependent on all the parameters. However, our inspection of the sign terms in the equations points out to the possibility of the existence of stable solutions, which indeed appear, as we will illustrate in the following section.

### III. COMPUTER SIMULATIONS

This section presents the results of simulations performed to illustrate the analytical results obtained in section II. We integrated numerically both the system of ordinary differential equations describing the evolution of the first two moments and multiple realisations of the stochastic model. In the case of equations (1) each experiment consists of 5000 simulations integrated using the Euler-Maruyama algorithm with a step size of  $h = 0.05$ . As stated earlier, the stimulus function was parabolic, the control function linear and the sensor noise additive, i.e. with constant variance. For all the simulation  $g_0 = 5$ ,  $a_{11} = a_{22} = 0.05$ ,  $g'_0 = 4.3$  and  $\alpha = 1.75$ . The differential equations (6) and (7) were integrated using the Runge-Kutta 4-5 algorithm with adaptive step size, which has a higher computational cost but also provides higher accuracy.

Figure 2 shows the evolution of the average  $x$  coordinate ( $\mu_x$ , bottom plot) over time and the four non-zero elements of the covariance matrix  $\sigma_{xx}$ ,  $\sigma_{yy}$ ,  $\sigma_{y\theta}$  and  $\sigma_{\theta\theta}$  for the case when  $g'_0 < g_0$ , which, as we can see, has a stable solution, i.e. bounded coefficients on the covariance matrix and the average  $x$  position. The dashed lines show the result of the numerical integration of the non-linear dynamical system (6) and (7), and the solid lines represents the values obtained for the mean and covariance for the trajectories

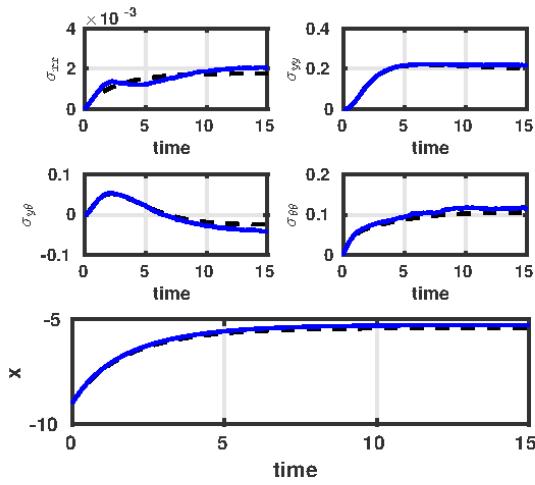


Fig. 2. Evolution of the average and elements of the covariance matrix (dashed line) and result of the simulation (solid line) for  $g'_0 < g_0$

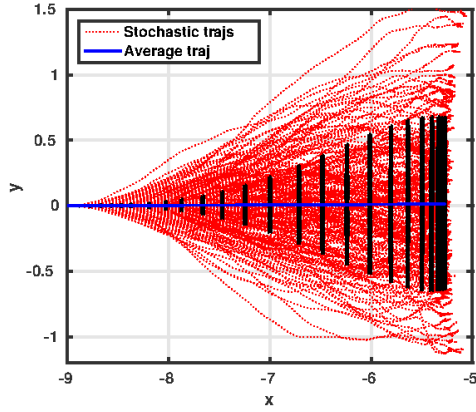


Fig. 3. Simulated trajectories and covariance matrices (black ellipses) for  $g'_0 < g_0$

simulated using equation (1). Figure 3 shows some of the corresponding simulations in the  $x$ - $y$  plane. The covariance matrix ( $3\sigma$  interval) is represented for some time stamps on the  $x$ - $y$  variables. It is worth noting that the time-steps for which the covariance matrix is plotted in figure 3 is logarithmic in scale, therefore the uncertainty ellipses (which look like lines because of the much higher dispersion on the  $y$  axis) are separated by exponentially increasing time intervals. Figure 3 shows that the average trajectory coincides with the expected deterministic trajectory, i.e. a straight line towards the stimulus maximum located at the origin. Since all the stochastic simulations start from the same point, the initial covariance matrix is zero, but it grows as the simulated vehicles move towards the maximum. It is worth noting that, the condition  $g'_0 < g_0$  was set to enforce the existence of a stable equilibrium on the system (6) and (7). Like in the case of the noiseless vehicle 3a, that condition entails that the average  $x$  position  $\mu_x$  will not reach the maximum of the stimulus, which also occurs for the case of noisy sensors. Figure 2 also shows that the elements of  $\Sigma$  converge to a stable equilibrium point, meaning that the variance of

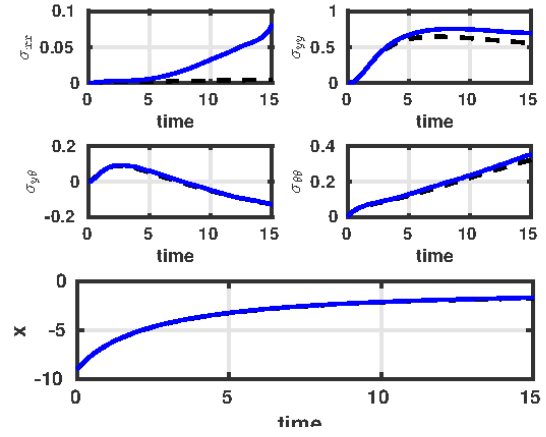


Fig. 4. Evolution of the average and elements of the covariance matrix (dashed line) and result of the simulation (solid line) for  $g'_0 = g_0$

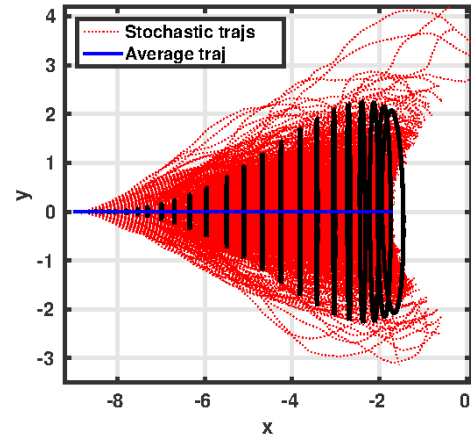


Fig. 5. Simulated trajectories and covariance matrices (black ellipses) for  $g'_0 = g_0$

the trajectories is bounded, as pointed by the analysis in section II-B.

Figures 4 and 5 show the results for a simulation with  $g'_0 = g_0$ , which could lead to instability of the equations (6) and (7). Interestingly, the trajectories shown in figure 5 converge to the origin and the average trajectory seems to be stable despite the absence of negative terms in equation (6) for the simulated time. Although the elements of the covariance matrix  $\dot{\sigma}_{yy}$ ,  $\dot{\sigma}_{y\theta}$  and  $\dot{\sigma}_{\theta\theta}$  match closely those of the stochastic simulations, there is a large divergence in the result for  $\dot{\sigma}_{xx}$  which grows linearly over time after 5 seconds. This divergence is due to the non-linearity of the stimulus function. Because the stimulus is a quadratic function the distributions of the simulated vehicles will deviate from a Gaussian distribution over time (it is worth reminding that the initial distribution of vehicles can be stated as  $p(x, y, \theta) = \delta(x+d)\delta(y)\delta(\theta)$  which corresponds to a Gaussian with zero covariance matrix). Therefore, although the approximate of the first two moments of the trajectories predict a bounded variation on the trajectories and convergence to the origin, the non-linearity of the stimulus makes the dispersion of the vehicles larger in the  $x$  direction.

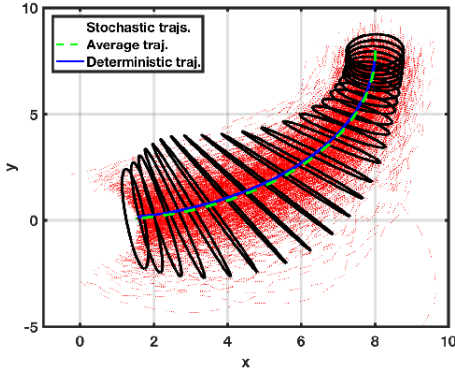


Fig. 6. Simulation of vehicles 3a starting outside the analytical solutions with  $g'_0 = g_0$  (black ellipses represent the covariance)

#### A. Evolution outside the analytical trajectories

This section presents simulations of the stochastic equations when an analytical average trajectory cannot be obtained, i.e. the average trajectory is not a straight line towards the source. Figure 6 shows the trajectories (dotted lines) of vehicles with noisy sensors starting from random poses drawn from a Gaussian distribution centred at  $[\mu_x, \mu_y] = [8, 8]$ . The solid line represents the trajectory of a vehicle with ideal sensors starting at the average initial pose, while the dashed line corresponds to the average of the trajectories with noisy sensors. Although these two latter plots look quite similar, there is a small difference due to the additional terms accounting for the variance of the trajectories which depend on the Hessian of  $S(\mathbf{x})$ . These terms do not affect in the case of the straight line trajectory of the previous section. The solid ellipses around the average trajectory correspond to the  $x$  and  $y$  components of the covariance matrix ( $3\sigma$  interval). Because all the initial poses do not coincide there is a non zero initial covariance, which grows and shrinks in different directions as the trajectories evolve. In the long term the average trajectory converges to the source and approaches a straight line, while the dispersion of the trajectories decreases in the  $y$  direction but increase in the  $x$  direction as in figures 4 and 5. Therefore, even if the trajectory starts outside the range of straight line solutions, because of the convergence properties close to the analytical solution, the long term behaviour will be similar to the one obtained in the previous section.

### IV. CONCLUSIONS AND FUTURE WORK

This work analysed the behaviour of Braitenberg vehicle 3a close to a stimulus source when the sensors present white Gaussian noise. Multiple experimental works used the qualitative Braitenberg models to implement source reaching in robots. Although stable controllers exist, our results show that care must be taken when designing the control function for real robots. Specifically, a stable controller for a noiseless vehicle could generate a stable average trajectory (over multiple trials) although the dispersion at the end point can be large for a fixed trajectory time. Stability of the trajectories

can be ensured when the parameters of the control function are tuned so that it will not actually reach the highest value (source) of the stimulus.

As we stated earlier, finding the equilibrium point of the second order approximate of the trajectories involves finding the roots of a high degree polynomial, yet since the order is lower than five, an analytical solution exists. That would provide a condition equation for stable trajectories relating the stimulus, the parameters of the controller, the morphological parameters of the vehicle, and the noise level, at least for a simple linear  $F(s)$  close enough to the source. Future work will focus on finding more general conditions under which the variance of the trajectories is bounded, as well as finding the boundary values. Reinforcement Learning can also be applied to learn appropriate control functions to minimise the effects of noise in the trajectories.

#### ACKNOWLEDGEMENTS

This work was supported by the Royal Society International Exchange Scheme under grant IE151293.

#### REFERENCES

- [1] X. Mao, "Stochastic stabilization and destabilization," *Systems & Control Letters*, vol. 23, no. 4, 1994.
- [2] I. Rañó, M. Khamassi, and K. Wong-Lin, "A drift diffusion model of biological source seeking for mobile robots," in *Proceedings of the 2017 IEEE Intl. Conf. on Robot. and Autom.*, 2017, pp. 3525–3531.
- [3] V. Braitenberg, *Vehicles. Experiments in synthetic psychology*. The MIT Press, 1984.
- [4] I. Rañó, "Biologically inspired navigation primitives," *Robot. and Auto. Sys.*, vol. 62, no. 10, pp. 1361–1370, 2014.
- [5] I. Rañó, A. Gómez-Eguíluz, and F. Sanfilippo, "Bridging the gap between bio-inspired steering and locomotion: A braitenberg 3a snake robot," in *Proceedings of the 2018 IEEE Intl. Conf. on Control, Automation, Robotics and Vision*, 2018.
- [6] T. Salumäe, I. Rañó, O. Akanyeti, and M. Kruusmaa, "Against the flow: A braitenberg controller for a fish robot," in *Proc. of the Intl. Conf. on Robot. and Autom.*, 2012, pp. 4210–4215.
- [7] I. Rañó, "A steering taxis model and the qualitative analysis of its trajectories," *Adaptive Behavior*, vol. 17, no. 3, pp. 197–211, 2009.
- [8] —, "Results on the convergence of braitenberg vehicle 3a," *Artificial Life*, vol. 20, no. 2, pp. 223–235, 2014.
- [9] A. J. Lilienthal and T. Duckett, "Experimental analysis of gas-sensitive Braitenberg vehicles," *Advanc. Robot.*, vol. 18, no. 8, pp. 817–834, 2004.
- [10] J. Gonzalez-Jimenez, J. Monroy, , and J. Blanco, "The multi-chamber electronic nosean improved olfaction sensor for mobile robotics," *Sensors*, vol. 6, no. 11, pp. 6145–6164, 2011.
- [11] B. Webb, *A Spiking Neuron Controller for Robot Phonotaxis*. The MIT/AAAI Press, 2001, pp. 3–20.
- [12] A. Horchler, R. Reeve, B. Webb, and R. Quinn, "Robot phonotaxis in the wild: a biologically inspired approach to outdoor sound localization," *Advanced Robotics*, vol. 18, no. 8, pp. 801–816, 2004.
- [13] R. Reeve, B. Webb, A. Horchler, G. Indiveri, and R. Quinn, "New technologies for testing a model of cricket phonotaxis on an outdoor robot," *Robot. and Auton. Sys.*, vol. 51, no. 1, pp. 41–54, 2005.
- [14] M. Bernard, S. N'Guyen, P. Pirim, B. Gas, and J.-A. Meyer, "Phonotaxis behavior in the artificial rat psikharpax," in *International Symposium on Robotics and Intelligent Sensors*, 2010.
- [15] D. Shaikh, J. Hallam, J. Christensen-Dalsgaard, and L. Zhang, "A Braitenberg lizard: Continuous phonotaxis with a lizard ear model," in *Proc. of the 3rd Intl. Work-Conf. on The Interplay Between Natural and Artificial Computation*, 2009, pp. 439–448.
- [16] V. Lebastard, F. Boyer, C. Chevallereau, and N. Servagent, "Underwater electro-navigation in the dark," in *Proc. of the Intl. Conf. on Robot. and Autom.*, 2012, pp. 1155–1160.
- [17] P. Reverdy, B. D. Ilhan, and D. Koditschek, "A drift-diffusion model for robotic obstacle avoidance," in *Proc. of the IEEE/RSJ Intl. Conf. on Intel. Robots and Systems*, 2015, pp. 6113–6120.